*J. Fluid. Mech.* (1982), *vol.* 124, *pp.* 335–345
*Printed in Great Britain*



# Jets rising and falling under gravity

By JEAN-MARC VANDEN-BROECK
AND JOSEPH B. KELLER†
Department of Mathematics, Stanford University, Stanford, CA 94305

(Received 11 May 1981 and in revised form 13 January 1982)

Steady two-dimensional jets of inviscid incompressible fluid, rising and falling under gravity, are calculated numerically. The shape of each jet depends upon a single parameter, the Froude number $\lambda = q_c(Qg)^{-\frac{1}{3}}$, which ranges from zero to infinity. Here $q_c$ is the velocity at the crest of the jet, i.e. the highest point of the upper surface, $Q$ is the flux in the jet, and $g$ is the acceleration of gravity. For $\lambda = \infty$ the jet is slender and parabolic. It becomes thicker as $\lambda$ decreases, and reaches a limiting form at $\lambda = 0$. Then there is a stagnation point at the crest, where the surface makes a 120° angle with itself. This angle is predicted by the same argument Stokes used in his study of water waves.

The problem is formulated as an integro-differential equation for the two free surfaces of the jet. This equation is discretized to yield a set of nonlinear equations, which are solved numerically by Newton's method. In addition, asymptotic results for large $\lambda$ are obtained analytically. Graphs of the results are presented.

## 1. Introduction

When a stream of water emerges from a nozzle aimed upwards at some angle from the vertical, the stream rises to a maximum height and then falls in a somewhat parabolic arc, as is shown in figure 1. We shall calculate the shape of this kind of jet numerically by assuming that the flow within it is steady, two-dimensional and irrotational, and that the fluid is incompressible and inviscid. We shall take account of gravity but neglect all other forces, such as surface tension and air resistance. We shall also assume that the nozzle is infinitely far away, so that the flow is bounded entirely by two free streamlines.

We shall see that the shape of the jet is determined solely by its dimensionless Froude number

$$\lambda = q_c (Qg)^{-\frac{1}{3}}. \tag{1.1}$$

Here $g$ is the acceleration of gravity, $Q$ is the flux in the jet and $q_c$ is the flow velocity at the highest point of the jet, i.e. at its crest. As $\lambda$ tends to infinity, the jet becomes slender and its profile tends to a parabola. This is to be expected if each particle of the fluid moves independently of the others. An outer asymptotic solution for large $\lambda$, which yields this profile and corrections to it, was obtained by Keller & Weitz (1957) and Keller & Geer (1973). We derive the corresponding inner asymptotic solution, valid near the crest, and compare it with our numerical results in figures 3(*a*), 4 and 5. The agreement constitutes a check on the analysis and on the numerical method.

As $\lambda$ decreases we find that the jet becomes thicker. The limiting jet, for $\lambda = 0$, has a stagnation point at its crest, and the upper surface of the jet has a 120° corner

† Also: Department of Mechanical Engineering, Stanford University.

there, as can be seen in figure 3(*d*). The fact that there must be such an angle at a stagnation point on the upper surface follows by the same argument used by Stokes in the case of water waves. Furthermore for $\lambda$ small, the flow near the crest is similar to that near the crest of the almost highest steady progressing water wave. Consequently this flow is described by the calculations that have been made for the water-wave case by Grant (1973), Longuet-Higgins & Fox (1977) and others.

Our results can be interpreted as if the flow emerged from a nozzle at some large finite distance from the crest, aimed at an angle $\theta$ above the horizontal. For a fixed nozzle width and flux, the Froude number $\lambda$ can be expressed as a decreasing function of $\theta$. Then the velocity $q_c$ at the crest decreases as $\theta$ increases until $q_c = 0$ at some limiting nozzle angle $\theta_{\max}$. For $\theta > \theta_{\max}$ we could construct a solution corresponding to the potential plane of figure 2(*a*) with an additional free boundary along some line $\psi = \psi_0$, $\phi > 0$ with $-\frac{1}{2} \leqslant \psi_0 \leqslant 0$. This would represent a jet that splits into two near the crest, with one part continuing forward and the other part being thrown backward. The fraction of the flux in the backward jet would be $-\psi_0$, which would increase from zero at $\theta = \theta_{\max}$ to one half at $\theta = \frac{1}{2}\pi$.

The reason we have not calculated these split-jet solutions is that we expect the backward jet to overlap the unseparated jet when the solution is mapped into the physical plane. This should happen very near the crest when $-\psi_0$ is small, i.e. when $\theta$ is just slightly above $\theta_{\max}$, because the backward jet will emerge with a very low velocity. As $-\psi_0$ increases, i.e. as $\theta$ increases, the overlap region will move away from the crest. When $-\psi_0 = \frac{1}{2}$, i.e. when the incident jet is vertical, there will be no overlap since the overlap region will have moved to infinity.

If the flow emerges from a nozzle at a finite distance from the crest, the solution will be physically meaningful if the overlap occurs further from the crest than the nozzle. Otherwise the solution will not be meaningful, which suggests that then there will be no steady solution of the flow problem.

In §2 we formulate the problem as an integro-differential equation for the jet surface. Then in §3 we present a numerical method for solving this equation. It employs discretization, which converts the equation into a set of nonlinear algebraic equations, and Newton's method for solving these equations. The results are discussed in §4. In appendix A an outer asymptotic expansion for the jet is constructed for large $\lambda$, valid away from the crest. In appendix B the corresponding inner expansion, valid near the crest, is found.

## 2. Formulation

Let us consider a steady two-dimensional jet bounded by the upper streamline $\psi = 0$ and the lower streamline $\psi = -Q$, as is indicated in figure 1. Here $\psi$ is the stream function of the potential flow within the jet, and $\phi$ is the corresponding potential function. We choose Cartesian coordinates with origin at the crest and with the positive $y$-axis pointing vertically upward, and we set $\phi = 0$ at the origin. We also assume that the jet is symmetric about the $y$-axis, so that $\phi = 0$ on the axis $y = 0$.

On the two surfaces of the jet the Bernoulli equation yields

$$\tfrac{1}{2}(\nabla\phi)^2 + gy = \tfrac{1}{2}q_c^2 \quad (\psi = 0, -Q). \tag{2.1}$$

We now introduce dimensionless variables by using $(Q^2/g)^{\frac{1}{3}}$ as the unit of length and $(Qg)^{\frac{1}{3}}$ as the unit of velocity. In these variables (2.1) becomes

$$(\nabla\phi)^2 + 2y = \lambda^2 \quad (\psi = 0, -1), \tag{2.2}$$

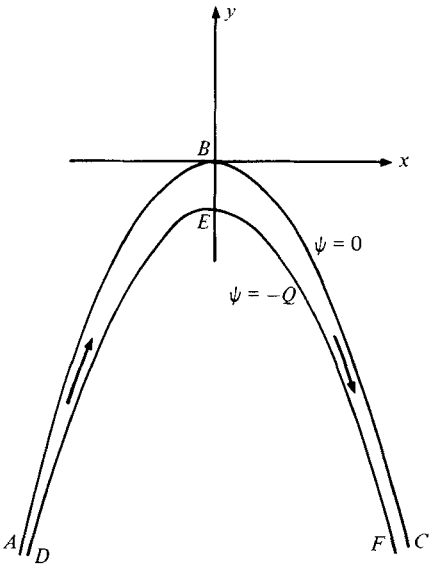


FIGURE 1. Sketch of the flow and of the coordinates.

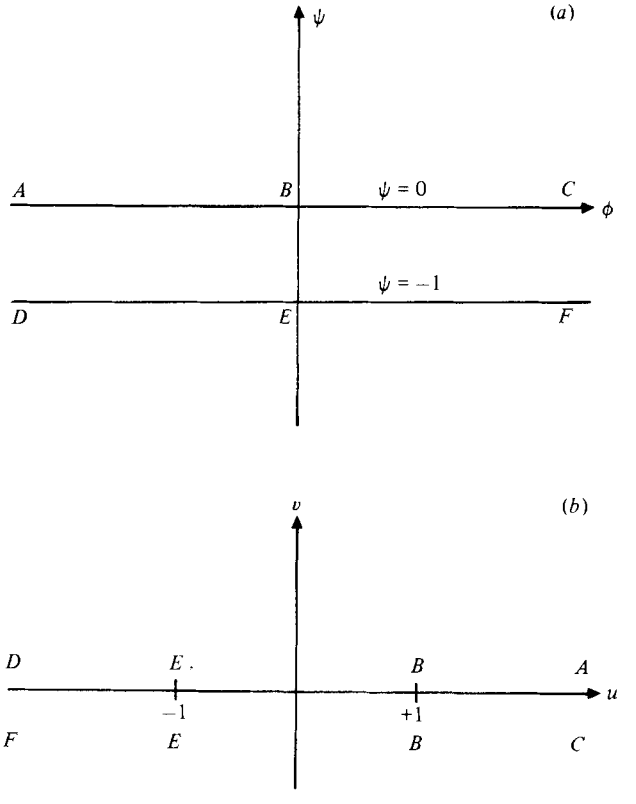


FIGURE 2. (*a*) The image of the flow is a strip in the plane of the complex potential $f = \phi + i\psi$. (*b*) The $w = u + iv$ plane.

where $\lambda$ is defined by (1.1). The problem is to find $z = x + iy$ as an analytic function of $f = \phi + i\psi$ in the strip $-1 \leqslant \psi \leqslant 0$ of the $f$-plane, with (2.2) holding on the boundaries of the strip. The strip in the $f$-plane is shown in figure 2(*a*).

It is convenient to map this strip onto the whole plane of the new complex variable $w = u + iv$ by the transformation

$$w = u + iv = \cosh \pi f. \tag{2.3}$$

The right half of the strip, indicated by *FEBC* in figure 2(*a*), is mapped onto the lower half of the $w$-plane shown in figure 2(*b*). The left half of the strip, *DEBA* in figure 2(*a*), is mapped onto the upper half of the $w$-plane in figure 2(*b*).

In view of (2.3), we now seek $z = z(w)$ as an analytic function of $w$ in the whole $w$-plane. When (2.2) is rewritten in terms of $x(u, v)$ and $y(u, v)$, only the values of $x(u, 0)$ and $y(u, 0)$ occur in it, since the two bounding streamlines are mapped onto the portions $|u| > 1$ of the axis $v = 0$. We shall therefore write $x(u) = x(u, 0)$ and $y(u) = y(u, 0)$. Then (2.2) becomes

$$2y(u) + [\pi^2(u^2 - 1)\{[x'(u)]^2 + [y'(u)^2]\}]^{-1} = \lambda^2 \quad (v = 0,\ |u| > 1). \tag{2.4}$$

Furthermore, $x = 0$ on the segment $BE$ of the $y$-axis in figure 1, which has been mapped onto the segment $BE$ of the $\psi$-axis in figure 2(*a*) and onto the segment $BE$ of the $u$-axis in figure 2(*b*). Therefore

$$x(u) = x(u, 0) = 0 \quad (|u| < 1). \tag{2.5}$$

The function $z'(w)$ is analytic in the lower half of the $w$-plane and tends to zero exponentially fast at infinity. Therefore, on $v = 0$, its imaginary part $y'(u)$ is the Hilbert transform of its real part $x'(u)$. From (2.5) $x'(u) = 0$ for $|u| < 1$, and thus the Hilbert transform yields

$$y'(u) = \frac{1}{\pi} \int_{-\infty}^{-1} \frac{x'(u')}{u' - u} du' + \frac{1}{\pi} \int_{1}^{\infty} \frac{x'(u')}{u' - u} du' \quad (-\infty < u < +\infty). \tag{2.6}$$

Next, since $B$ is at the origin in the $(x, y)$-plane and at $u = 1$, $v = 0$ in the $w$-plane, we have

$$y(1) = y(1, 0) = 0. \tag{2.7}$$

Now the $y$-coordinate of any point on the free surface, which corresponds to $(u, 0)$ in the $w$-plane, can be calculated by using (2.7) as an initial value and integrating $y'(u)$ to get

$$y(u) = \int_{1}^{u} y'(u)\, du. \tag{2.8}$$

For any value of $\lambda \geqslant 0$, (2.4), (2.6) and (2.8) are a set of equations for $x'(u)$, $y'(u)$ and $y(u)$. By using (2.6) and (2.8) to eliminate $y'(u)$ and $y(u)$, we can convert (2.4) into a single integro-differential equation for $x'(u)$ in the region $|u| > 1$. Once this equation is solved, $y'(u)$ can be found from (2.6), $y(u)$ can be found from (2.8), and $x(u)$ can be found by integrating $x'(u)$ with the initial condition (2.5). Then $x(u)$, $y(u)$ is a parametric representation of the two free surfaces of the jet. The range $u > 1$ gives the upper surface and the range $u < -1$ gives the lower surface.

## 3. Numerical method

Before solving (2.4), (2.6) and (2.8), we note that $z'(u) \sim (u^2-1)^{-\frac{1}{2}}$ near $u = \pm 1$, so that $z'(u)$ is singular at these two points. To remove these singularities we introduce the following new variables:

$$u = 1+\alpha^n \quad (u > 1,\ \alpha > 0), \tag{3.1}$$

$$u = -1-\beta^n \quad (u < -1,\ \beta > 0), \tag{3.2}$$

$$u = \cos \pi\delta \quad (-1 < u < +1,\ 0 < \delta < 1). \tag{3.3}$$

Here $n \geqslant 2$ is an integer to be chosen. Then the new functions $z(\alpha) = z[u(\alpha)]$, $z(\beta) = z[u(\beta)]$ and $z(\delta) = z[u(\delta)]$ have derivatives that are finite everywhere. Therefore we rewrite (2.4), (2.6) and (2.8) in terms of $\alpha$, $\beta$, $\delta$, $z(\alpha)$, $z(\beta)$ and $z(\delta)$.

Next we introduce the mesh points

$$\alpha_I = \tfrac{1}{2}(2I-1)\,E \quad (I = 1, \ldots, N_1-1), \tag{3.4}$$

$$\beta_I = \alpha_I \quad (I = 1, \ldots, N_1-1), \tag{3.5}$$

$$\delta_I = (2I-1)/2N_2 \quad (I = 1, \ldots, N_2). \tag{3.6}$$

Here $E$ is the mesh width. We also define the $2N_1-2$ unknowns

$$X'(\alpha_I) = X_\alpha(\alpha_I) \quad (I = 1, \ldots, N_1-1), \tag{3.7}$$

$$X'(\beta_I) = X_\beta(\beta_I) \quad (I = 1, \ldots, N_1-1). \tag{3.8}$$

In addition we shall use the intermediate mesh points

$$\alpha_{I+\frac{1}{2}} = \tfrac{1}{2}(\alpha_I+\alpha_{I+1}) \quad (I = 1, \ldots, N_1-2), \tag{3.9}$$

$$\beta_{I+\frac{1}{2}} = \alpha_{I+\frac{1}{2}} \quad (I = 1, \ldots, N_1-2). \tag{3.10}$$

Then we compute $Y'(\alpha_{I+\frac{1}{2}})$, $Y'(\beta_{I+\frac{1}{2}})$ and $Y'(\delta_I)$ in terms of the $X'(\alpha_I)$ and $X'(\beta_I)$ by applying the trapezoidal rule to the integrals in (2.6), rewritten in terms of the new variables, with the mesh points $\alpha_J$ and $\beta_J$. The symmetric spacing of the mesh points enables us to compute the Cauchy principal-value integrals as if they were ordinary integrals. (For more details see Vanden-Broeck & Schwartz 1979; Vanden-Broeck & Keller 1980.)

Next we use the values of $Y'(\alpha_I)$ in (2.8) to compute $Y(\beta)|_{\beta=0}$. From (2.8) we have $Y(\alpha)|_{\alpha=0} = 0$. We then use the values of $Y'(\alpha_{I+\frac{1}{2}})$ and $Y'(\beta_{I+\frac{1}{2}})$ to compute $Y(\alpha_I)$ and $Y(\beta_I)$ from (2.8) by the trapezoidal rule, and to find $Y'(\alpha_I)$ and $Y'(\beta_I)$ by interpolation. The error inherent in approximating the infinite integrals by finite integrals should be negligible for $N_1E$ large enough. This was found to be the case in the computations to be described.

By proceeding in this way, we obtain $Y'(\alpha_I)$, $Y(\alpha_I)$, $Y(\beta_I)$ and $Y'(\beta_I)$ in terms of $X'(\alpha_I)$ and $X'(\beta_I)$. We then substitute these values into (2.6) at the mesh points $\alpha_I$, $\beta_I$ $(I = 1, \ldots, N_1-2)$. Thus we obtain $2N_1-4$ equations for the $2N_1-2$ unknowns $X'(\alpha_I)$, $X'(\beta_I)$. The last two equations are obtained by expressing $X'(\alpha_{N_1-1})$ and $X'(\beta_{N_1-1})$ in terms of $X'(\alpha_I)$ and $X'(\beta_I)$ $(I = N_1-4, \ldots, N_1-2)$ by three-point Lagrange formulas.

For a given value of $\lambda$ we solved this system by Newton's method. In most of the computations we used $n = 5$, $N_1 = 20$, $N_2 = 20$ and $E = 0{\cdot}2$. Numerical tests were performed by increasing $N_1$ and $N_2$ and varying $E$ to check that the results obtained were correct to at least graphical accuracy.

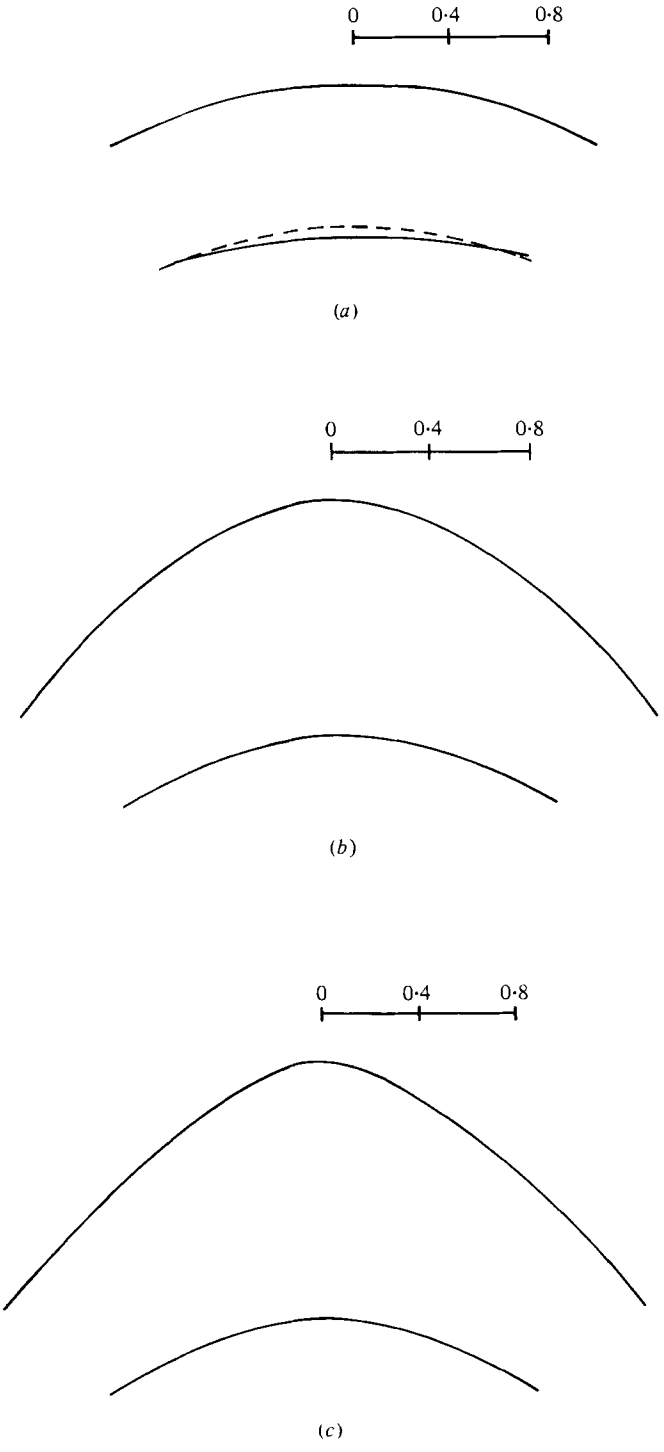


FIGURE 3(a)–(c). For caption see facing page.

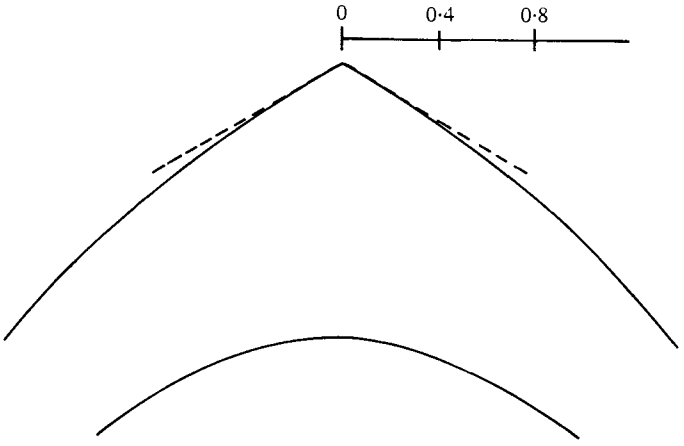


(*d*)

FIGURE 3. Profiles of the jet computed numerically for four values of $\lambda$: (*a*) $\lambda = 1{\cdot}4$; (*b*) 0·6; (*c*) 0·4; (*d*) 0. The horizontal and vertical scales are the same. In case (*a*) the top surface coincides, to graphical accuracy, with the parabola $y = -x^2/2\lambda^2$ obtained by eliminating $x_0$ from the first terms of (4.1) or eliminating $\phi$ from the first terms of (4.3). The dashed curve in (*a*) is the parabola $y = -\lambda^{-1} + \frac{1}{2}\lambda^4 - x^2/2\lambda^2$, obtained by eliminating $\phi$ from the first two terms (up to $\lambda^{-4}$) in (4.4). The dashed lines in (*d*) correspond to the Stokes angle of 120°.

## 4. Discussion of the results

We have used the numerical scheme of §3 to compute solutions for various values of $\lambda$. We started with a large value of $\lambda$ and used a uniform stream as the initial guess. After the solution converged, it was used as the initial guess for a smaller value of $\lambda$, and so on. Profiles for $\lambda = 1{\cdot}4$, 0·6, 0·4 and 0 are shown in figure 3.

In order to compare our computed results with analytical ones, we have solved the flow problem asymptotically for large $\lambda$. First (see appendix A) we used the theory of Keller & Geer (1973) to get the following asymptotic results for the jet's surfaces in terms of the parameter $x_0$. For the upper surface we get

$$x = \tfrac{1}{2}\lambda^2\{x_0 - \lambda^{-3}x_0[(1-\tfrac{1}{4}x_0^2)(4+x_0^2)^{-1} - \tfrac{1}{4}] + O(\lambda^{-6})\} \tag{4.1a},$$

$$y = \tfrac{1}{2}\lambda^2\{-\tfrac{1}{4}x_0^2 - 2\lambda^{-3}[(1-\tfrac{1}{4}x_0^2)(4+x_0^2)^{-1} - \tfrac{1}{4}] + O(\lambda^{-6})\} \tag{4.1b}$$

For the lower surface we find

$$x = \tfrac{1}{2}\lambda^2\{x_0 - \lambda^{-3}x_0[(5-\tfrac{1}{4}x_0^2)(4+x_0^2)^{-1} - \tfrac{1}{4}] + O(\lambda^{-6})\}, \tag{4.2a}$$

$$y = \tfrac{1}{2}\lambda^2\{-\tfrac{1}{2}x_0^2 - 2\lambda^{-3}[(5-\tfrac{1}{4}x_0^2)(4+x_0^2)^{-1} - \tfrac{1}{4}] + O(\lambda^{-6})\}. \tag{4.2b}$$

Although these equations seem to describe the jet everywhere, they actually yield an outer expansion, valid away from the crest. We see this by examining (4.2*b*), in which the second term exceeds the first term when $|x_0| \lesssim (8/\lambda^3)^{\frac{1}{2}}$, which corresponds to $|x| \lesssim (2\lambda)^{\frac{1}{2}}$. Therefore in appendix B we derive an inner expansion for the flow in the jet and for its surfaces, valid in the neighbourhood of $x = 0$. The resulting parametric equations for the upper surface are

$$x = \frac{\phi}{\lambda} - \frac{\phi^3}{3\lambda^7} + O(\lambda^{-10}), \tag{4.3a}$$

$$y = \frac{-\phi^2}{2\lambda^4} + \frac{\phi^2}{2\lambda^7} + O(\lambda^{-10}), \tag{4.3b}$$

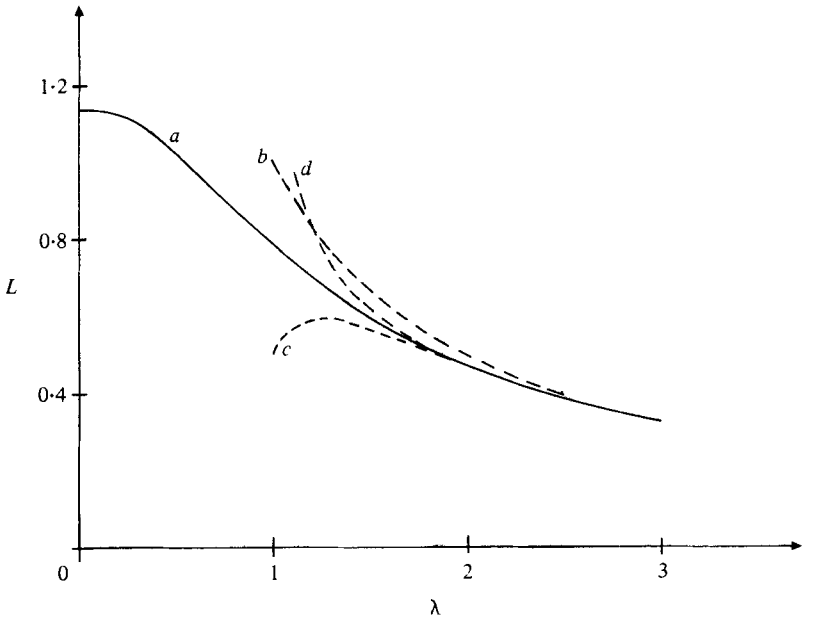


FIGURE 4. Thickness of the jet as a function of the Froude number $\lambda$. The curve ($a$) corresponds to the numerical results. The curves ($b$), ($c$) and ($d$) corresponds respectively to one, two and three terms of the asymptotic forumula (4.5).

and for the lower surface they are

$$x = \frac{\phi}{\lambda} - \frac{\phi}{\lambda^4} + \frac{\phi}{\lambda^7} - \frac{\phi^3 - 3\phi}{3\lambda^7} + O(\lambda^{-10}), \tag{4.4a}$$

$$y = \lambda^{-1} - \frac{\phi^2 - 1}{2\lambda^4} + \frac{\phi^2 - 1}{2\lambda^7} + \frac{3\phi^2 - 1}{3\lambda^7} + O(\lambda^{-10}). \tag{4.4b}$$

The asymptotic results (4.3$a$, $b$) and (4.4$a$, $b$) are compared with the numerical results for the jet with $\lambda = 1{\cdot}4$ in figure 3($a$).

The jet thickness $L$ at the crest is the difference between the values of $y$ given by (4.3$b$) and (4.4$b$) at $x = \phi = 0$. It is given by

$$L = \lambda^{-1} - \tfrac{1}{2}\lambda^{-4} + \tfrac{5}{6}\lambda^{-7} + O(\lambda^{-10}). \tag{4.5}$$

The first term in (4.5) is given by Keller & Weitz (1957), and the first two terms also follow from the outer expansion (4.1$a$, $b$) and (4.2$a$, $b$). In figure 4 we present our numerical results for $L$ and compare them with (4.5). For $\lambda > 1{\cdot}5$ the first term agrees with the numerical results within 12%, and two terms agree within 4%.

A measure of the variation in the flow velocity across the jet is the ratio $B$ of the square of the velocity at the crest to the square of the velocity at the point on the lower surface directly beneath the crest. From Bernoulli's equation $B$ is given by

$$B = \frac{\lambda^2}{\lambda^2 + 2L}. \tag{4.6}$$

In figure 5 we show $B$ as a function of $\lambda$ based upon our numerical results. For comparison we also show the value of $B$ given by the asymptotic theory of appendix B, obtained by using (4.5) for $L$ in (4.6).

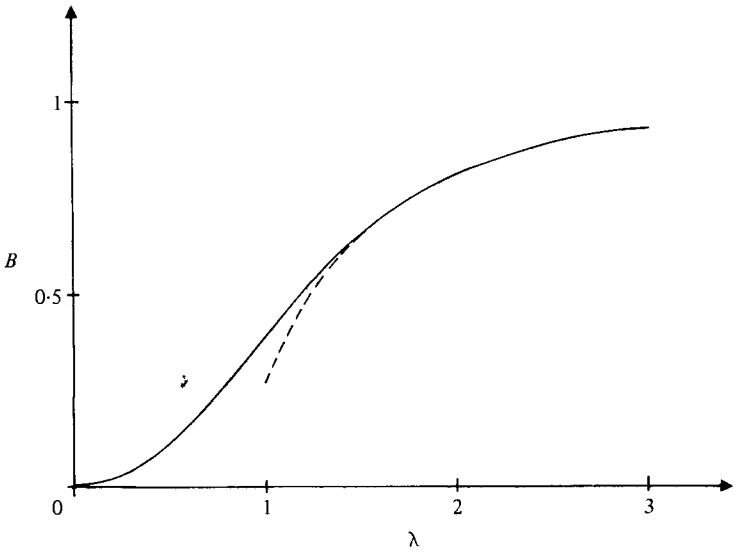


FIGURE 5. The ratio $B$ of the square of the velocity at the crest to the square of the velocity at the point beneath the crest on the lower surface, given by (4.6), as a function of $\lambda$. The solid curve is based upon the numerical results and the dashed curve is obtained by using the asymptotic result (4.5) for $L$ in (4.6).

We have computed solutions for $\lambda$ up to and including the limiting case $\lambda = 0$ shown in figure 3(*d*), at which a stagnation point occurs at the crest on the upper surface of the jet. The flow in the neighbourhood of such a point can be found analytically by employing the argument used by Stokes (1880) in the case of water waves, which yields

$$z(f) \sim (\tfrac{9}{4})^{\frac{1}{3}} f^{\frac{2}{3}} e^{-i\pi/6} \quad \text{as} \quad f = \phi + i\psi \to 0. \tag{4.7}$$

From (4.7) it follows that the surface has a 120° corner at the stagnation point. The broken lines in figure 3(*d*) enclose a 120° angle with its vertex at the crest. We see that these lines are tangent to the free surface there, which shows the agreement between the numerical solution and the local result (4.7).

To compute the jet shown in figure 3(*d*) we used $n = 6$ in the change of variables (3.1) and (3.2). We did so because for this choice of $n$ it follows from (4.5) that $z_\alpha(\alpha) = \alpha + o(\alpha)$ as $\alpha \to 0$ and that $z_\beta(\beta) = \beta + o(\beta)$ as $\beta \to 0$.

Correction terms to (4.7) for the highest steady periodic gravity wave were obtained by Grant (1973), and for almost-highest waves they were found by Longuet-Higgins & Fox (1977). Those terms also apply to the jet with $\lambda = 0$ and $\lambda$ near zero, respectively. They show that the surface undulates slightly near the crest. Longuet-Higgins & Fox (1977) found that these undulations were accompanied by an oscillation in the velocity of the waves as a function of their steepness, with infinitely rapid oscillations occurring as the steepness approaches its maximum value. Therefore we expect similar oscillations in figure 4, which would imply that $L$ oscillates infinitely often as $\lambda \to 0$. These oscillations would be of an amplitude too small to be seen on the scale of figure 4, and smaller than the numerical accuracy of the present work. One consequence of such oscillations might be that the highest two-dimensional jet is not the thickest.

## Appendix A. Outer expansion

We shall now apply to the present problem the theory of slender jets given by Keller & Geer (1973). To do so we choose the unit of velocity to be $q_c$ and unit of length to be $q_c^2/2g$. Then the parameters $\gamma$ and $\epsilon$ introduced by Keller & Geer (their equation (2.1)) become $\gamma = 1$ and $\epsilon = 2\lambda^{-3}$. The first terms in their expansions (3.1) and (3.2) become

$$z(\phi + i\psi, 2\lambda^{-3}) = z_0(\phi) + 2\lambda^{-3}[z_0'(\phi)\, i\psi + z_1(\phi)] + 4\lambda^{-6}[\tfrac{1}{2}z_0''(\phi)\,(i\psi)^2 + z_1'(\phi)\, i\psi + z_2(\phi)] + O(\lambda^{-9}). \tag{A 1}$$

Now $z_0 = x_0 + iy_0$ is given by their equations (3.18) and (3.19), with $y_0(0) = a = 0$ and $dy_0(0)/dx_0 = \tan\beta = 0$, corresponding to the fact that the origin is at the crest of the jet. Then their (3.20) yields $b = \frac{1}{4}$, so that (3.18) and (3.19) lead to

$$y_0 = -\tfrac{1}{4}x_0^2, \tag{A 2}$$

$$\phi = x_0 + \tfrac{1}{12}x_0^3. \tag{A 3}$$

Next, by setting $y_1(0) = 0$ and $y_1'(0) = 0$, we find from (3.34) and (3.35) of Keller & Geer that $A_1 = 0$ and $B_1 = -\frac{1}{4}$. Then their (3.32) and (A 2) above yield

$$y_1 = -(1 - \tfrac{1}{4}x_0^2)\,(4 + x_0^2)^{-1} + \tfrac{1}{4}. \tag{A 4}$$

With $x_1 = 0$, then their (3.33) gives

$$x_1(\phi) = \tfrac{1}{2}x_0(\phi)y_1(\phi). \tag{A 5}$$

By using (A 2)–(A 5) in (A 1) at $\psi = 0$ and at $\psi = -1$, we obtain the equations of the upper and lower surfaces of the jet in the parametric forms (4.3) and (4.4) respectively. The unit of length in the text is $(Q^2/g)^{\frac{1}{3}}$, which is $2\lambda^{-2}$ times that used in this appendix, namely $q_c^2/2g$. Therefore the expressions for $x$ and $y$ have been multiplied by $\frac{1}{2}\lambda^2$ to convert them to the units used in the text.

The jet thickness $L$ beneath the crest can be found by subtracting $y$ given by (4.3) from $y$ given by (4.4) at $x_0 = 0$. In the units of this appendix this yields $L = 2\lambda^{-3} + O(\lambda^{-6})$. The next term can be found by keeping the terms of order $\lambda^{-6}$ in (A 1). By using the fact that $x_0'(0) = 0$ and $y_0''(0) = -\frac{1}{2}$, we get in this way

$$\begin{aligned} L &= 2\lambda^{-3} + 4\lambda^{-6}[\tfrac{1}{2}y''(0) + x_1'(0)] + O(\lambda^{-9}) \\ &= 2\lambda^{-3} - \lambda^{-6} + O(\lambda^{-9}). \end{aligned} \tag{A 6}$$

In the units used in the text, $L$ is given by the first two terms in (4.5).

## Appendix B. Inner expansion

As was pointed out in the text, the expansion given in appendix A is not valid near the crest, so we shall now construct another expansion, which is valid there. To do so we choose the unit of velocity to be $q_c$ as before, but now we choose the unit of length to be $Q/q_c$, where $Q$ is the mass flux in the jet. Then the Bernoulli equation on the surfaces of the jet becomes

$$q^2 + 2\epsilon y = 1 \quad (\psi = 0, -1). \tag{B 1}$$

Here $\epsilon = \lambda^{-3} = Qg/q_c^3$. We seek a function $z(\phi + i\psi) = x(\phi, \psi) + iy(\phi, \psi)$, analytic in the strip $-1 \leqslant \psi \leqslant 0$, and which satisfies (B 1) on the boundaries of the strip. In terms of $z$, (B 1) becomes

$$(x_\phi^2 + y_\phi^2)^{-1} + 2\epsilon y = 1 \quad (\psi = 0, -1). \tag{B 2}$$

In addition we require $\phi = \psi = 0$ at $x = y = 0$.

To solve (B 2) we write

$$z(\phi + i\psi) = z_0(\phi + i\psi) + \epsilon z_1(\phi + i\psi) + \epsilon^2 z_2(\phi + i\psi) + \ldots. \tag{B 3}$$

Then we use (B 3) in (B 2) and equate coefficients of corresponding powers of $\epsilon$. This leads to a sequence of problems for $z_0$, $z_1$, etc., the first of which is

$$(x_{0\phi}^2 + y_{0\phi}^2)^{-1} = 1 \quad (\psi = 0, -1), \tag{B 4}$$

$$x_0 = y_0 = 0 \quad (\phi = \psi = 0). \tag{B 5}$$

The only analytic function satisfying (B 4) and (B 5) and growing slower than an exponential at infinity is $z_0 = \phi + i\psi$, so that $x_0 = \phi$ and $y_0 = \psi$.

The boundary condition (B 2) yields at order $\epsilon$

$$x_{1\phi} = \psi \quad (\psi = 0, -1). \tag{B 6}$$

We can satisfy (B 6) by requiring $z_1' = -i(\phi + i\psi)$, so that $z_1 = -\frac{1}{2}i(\phi + i\psi)^2$. This is the unique solution for $z_1$ that vanishes at the origin and grows more slowly than an exponential at infinity. From (B 2) at order $\epsilon^2$ we get

$$x_{2\phi} = 2\psi^2 - \phi^2 \quad (\psi = 0, -1). \tag{B 7}$$

We find that $z_2 = \frac{1}{2}i(\phi + i\psi)^2 - \frac{1}{3}(\phi + i\psi)^3$.

On collecting our results we obtain

$$x + iy = \phi + i\psi - \frac{i}{2\lambda^3}(\phi + i\psi)^2 + \frac{1}{\lambda^6}[\tfrac{1}{2}i(\phi + i\psi)^2 - \tfrac{1}{3}(\phi + i\psi)^3] + O(\lambda^{-9}). \tag{B 8}$$

The results (4.3) and (4.4) follow from (B 8) by setting $\psi = 0$ and $\psi = -1$ respectively, and separating real and imaginary parts.

This research was supported in part by the Army Research Office, the Office of Naval Research, the Air Force Office of Scientific Research, and the National Science Foundation.

## REFERENCES

GRANT, M. A. 1973 *J. Fluid Mech.* **59**, 257.

KELLER, J. B. & GEER, J. 1973 *J. Fluid Mech.* **59**, 417.

KELLER, J. B. & WEITZ, M. L. 1957 In *Proc. 9th Int. Congr. Appl. Mech., Brussels*, vol. 1, p. 316.

LONGUET-HIGGENS, M. S. & FOX, M. J. H. 1977 *J. Fluid Mech.* **80**, 721.

VANDEN-BROECK, J.-M. & KELLER, J. B. 1980 *J. Fluid Mech.* **98**, 161.

VANDEN-BROECK, J.-M. & SCHWARTZ, L. W. 1979 *Phys. Fluids* **22**, 1868.

STOKES, G. G. 1880 In *Mathematical and Physical Papers*, vol. 1, p. 225.